

**RESEARCH**

# Comparative Study of the Photothermal Behavior of Polydopamine-, Polypyrrole-, and Carbon Nanotubes-based Materials

Gabriela Herrera-Rodríguez<sup>1</sup> | Andya J. Ramírez Irigoyen<sup>1</sup> | Karla F. García Verdugo<sup>1</sup> | Ana V. Torres Figueroa<sup>1</sup> | Brianda M. Salazar Salas<sup>1</sup> | José C. Encinas-Encinas<sup>1</sup> | Cinthia J. Pérez-Martínez<sup>2,\*</sup>  | Teresa del Castillo-Castro<sup>1,\*</sup> 

<sup>1</sup>Departamento de Investigación en Polímeros y Materiales, Universidad de Sonora, Hermosillo 83000, Sonora, Mexico

<sup>2</sup>Departamento de Ciencias Químico Biológicas, Universidad de Sonora, Hermosillo 83000, Mexico

\*Corresponding authors:  
E-mail: jhovanna.perez@unison.mx  
(Cinthia J. Pérez-Martínez)  
teresa.delcastillo@unison.mx  
(Teresa del Castillo Castro)  
Tel.: +52-66-22-59-21-63  
+52-66-22-59-21-61

## ABSTRACT

The development of conjugated polymer- and carbonaceous-based platforms as NIR photothermal materials is a valuable contribution to modern-day cancer therapies. Measurements of the thermal response of these materials under same NIR irradiation conditions allows accurately comparing their photothermal capacities to accomplish specific biomedical requirements. In this work, polydopamine (PDA) and polypyrrole (PPy) nanoparticles were synthesized by green-based methods and their photothermal behavior, compared to that of acid-treated carbon nanotubes (CNT), was studied under the same experimental setup. Furthermore, PDA, PPy, and CNT nanostructures were embedded within a crosslinked poly(N-isopropylacrylamide-*co*-acrylic acid) (P(NIPAM-*co*-AA)) matrix, and the photothermal properties of these novel nanocomposite hydrogels were also comparatively studied. Experimental conditions such as the filler concentration, irradiation time, and laser power, as well as the nanocomposite hydrogel composition can be tuned to yield mild (39–43 °C) or high (47–50 °C) hyperthermia conditions, as required. The photothermal results of P(NIPAM-*co*-AA) nanocomposite hydrogels containing PDA, PPy, or CNT nanostructures evidenced the potential of these materials in controlled drug delivery and for combined chemo-photothermal therapies of tumors by NIR laser irradiation.

## KEYWORDS

Photothermal effect, nanocomposite hydrogel, polymer nanoparticles.

## INTRODUCTION

Photothermal effect is the phenomenon of converting light energy into thermal energy by photothermal agents under light irradiation [1]. In recent years, scientific research has shown the potential use of photothermal agents in solar-driven water vaporization technologies [2], environmental and catalytic applications [3], and wastewater treatments [4], as well as in the biomedical field as part of controlled drug release systems [5], and for photothermal therapy (PTT) purposes [6].

The PTT typically employs near-infrared radiation (NIR) due to its minimal absorption by hemoglobin and water, safe effect on biological tissues, and deep tissue

penetration [7,8]. Numerous efforts have been made to develop bioactive nanomaterials with high NIR photothermal conversion efficiency [9]. Photothermal materials are currently classified into four categories: metallic nanostructures (e.g., Au [10] and Ag nanoparticles [11]), inorganic semiconductor materials [4], carbon-based nanomaterials [12], and organic molecules (e.g. polymers) [1,2,13].

Heavy metal nanoparticles have been the first-line option for PTT uses owing to their favorable absorbance properties, high photothermal conversion efficiency, and suitable photo-stability. However, inorganic materials are non-biodegradable and may remain within the body for

long periods, leading to their accumulation in organs and tissues with potential toxicity concerns [13,14].

On the other hand, carbonaceous nanomaterials like carbon nanotubes (CNT) may induce cytotoxicity and some health complications, including the generation of reactive oxygen species and pulmonary inflammation [14–16]. In this regard, the formation of CNT complexes with bioactive species has been explored to improve its biocompatibility and exploit its valuable properties in PTT applications [12,17].

The assessment of polymer nanoparticles as photothermal agents has been growing in last years. Polymer materials stand out by their synthetic flexibility, biodegradability, and low cytotoxicity effects, overcoming the limitations associated with traditional photothermal systems [6,13]. For example, Bang-Ping et al. synthesized non-cytotoxic hyaluronic acid-polyaniline nanoparticles that showed an excellent behavior in photothermal ablation of HeLa and HCT-116 cancer cells [18]. In a similar approach, Li *et. al.* prepared polypyrrole (PPy) nanoparticles functionalized with polydopamine (PDA) that were successfully used in the photothermal ablation of HeLa tumor models and HeLa cells [19].

The incorporation of photothermal agents into suitable hydrogels allows obtaining multifunctional nanocomposite materials with several additional attributes such as mechanical flexibility, elasticity, adhesiveness, and biocompatibility [20–22]. In this regard, Wang *et. al.* [23] reported the entrapment of PDA nanoparticles within a poly(ethylene glycol) hydrogel for combined chemo-photothermal therapy. Geng *et. al.* [24] developed a novel injectable photothermal hydrogel based on poly(acrylic acid-*b*-N-isopropylacrylamide-*b*-acrylic acid) and PPy with high doxorubicin loading capacity and controlled/sustained drug release behavior upon NIR laser irradiation.

Overall, independent studies have shown the potential of conjugated polymer as photothermal agents for NIR-mediated therapeutic uses. However, studies focused on the comparison of photothermal efficiencies of different polymer systems under same experimental conditions are scarce in literature. These studies are important to qualify comparatively the photothermal behavior of materials without the effect of some experimental variables and measurement set-up.

In this work, the photothermal behavior of PDA nanoparticles, PPy colloids, and CNT in aqueous suspension was assessed under an identical experimental set-up and using similar measurement conditions (concentration, radiation wavelength, NIR radiation power, and irradiation time). Furthermore, PDA, PPy, and CNT nanostructures were embedded within a crosslinked poly(N-isopropylacrylamide-*co*-acrylic acid) (P(NIPAM-*co*-AA)) matrix, and the photothermal behavior of the nanocomposite hydrogels was also comparatively discussed.

## EXPERIMENTAL

### Materials

Dopamine hydrochloride (DA, 98 %), pyrrole (Py, 98 %), hydrogen peroxide (H<sub>2</sub>O<sub>2</sub>, 50 wt %), sodium taurocholate hydrate (Tch, ≥ 97 %), multiwalled carbon nanotubes (MWCNT, ≥ 98 %, OD × ID × L: 10 nm ± 1 nm × 4.5 nm ± 0.5 nm × 3–6 μm), acrylic acid (AA, 99 %), N,N,N',N'-tetramethylethylenediamine (TEMED, 99 %), potassium persulfate (KPS, ≥ 99 %), N,N'-methylenebisacrylamide (NMBA, 99 %) were purchased from Sigma Aldrich. N-isopropylacrylamide (NIPAAm, 97 %) was obtained from Alfa Aesar. Py monomer was distilled under vacuum and stored in dark at about -15 °C prior to use. All other reagents were of analytical grade and used as received without further purification. The aqueous solutions were prepared with deionized water, purified by a Milli-Q Organex system (Millipore, Molsheim, France).

### Synthesis of PDA nanoparticles

PDA nanoparticles were synthesized by the auto-polymerization of DA in alkaline aqueous media. DA 1 mM solution was prepared in 60 mL of water:EtOH solvent mixture in a volume ratio of 5:1. Then, the monomer solution was basified using the trizma buffer (pH 8.5, 100 mM) and kept under stirring (500 rpm) for 24 h at 60 °C. The product was carefully transferred to dialysis tubing (cellulose acetate, molecular mass cutoff of 6 kDa) and dialyzed against milliQ water for removing unreacted monomer molecules. Finally, PDA nanoparticles were dried by lyophilization using a vacuum freeze dryer 4.5 L Labconco FreeZone device.

### Synthesis of PPy colloids

PPy colloids were synthesized by the emulsion technique using Tch as biosurfactant, as previously reported our research group [25]. Briefly, a solution of Tch (10.5 mM) was prepared in 26 mL of citrate buffer (100 mM, pH 3.0). The resulting Tch solution was kept under stirring for 1 h, and then, Py (800 mM) was incorporated into the emulsion with further stirring for 2 h. The polymerization started by adding H<sub>2</sub>O<sub>2</sub> (800 mM). After 24 h of reaction, the product was rinsed three times with milliQ water through centrifugation for 1 h at 12,500 rpm.

### Functionalization of multi-walled carbon nanotubes

CNT used in all experiments were previously functionalized by acid treatment. Briefly, CNT were treated in a mixture of HNO<sub>3</sub>:H<sub>2</sub>SO<sub>4</sub> (3:1 volume ratio), as previously reported Quevedo *et. al.* [26]. In a typical experiment, 10 mg of pristine CNT were added to 10 mL of the acid mixture and kept under stirred for 4 h at 80 °C. Then, the mixture was refluxed at room temperature for 4 h. Finally, the product was purified by dialysis against milliQ water using cellulose acetate membranes (molecular mass cutoff of 6 kDa).

## Preparation of P(NIPAM-co-AA) nanocomposite hydrogels

Nanocomposite hydrogels were prepared by the copolymerization/reticulation of NIPAM and AA in the presence of different concentrations of PDA, PPy, or CNT nanostructures. Co-monomer amounts of 7.71 mmol of NIPAM, 1.38 mmol of AA, and 0.35 mmol of NMBA were dissolved in 10 mL of milliQ water, in a three-necked flask equipped with a nitrogen gas inlet. The monomer mixture was stirred for 30 min in nitrogen atmosphere. A proper amount of the filler (PDA, PPy, or CNT) was added to the monomer solution. Then, 0.74 mmol of KPS, previously dissolved in 5 mL of milliQ water, were added to the former solution to initiate the polymerization/reticulation process. After 15 min, 0.5 mL of the reaction mixture were mixed with 10  $\mu$ L of TEMED reactant (accelerator) in a container chilled in ice bath (4 °C). Next, the resultant mixture was poured into 5 mm internal diameter and 2 cm high cylindrical mold for gelation. Finally, hydrogels were washed with milliQ water and freeze-dried by lyophilization. Hydrogel samples were identified in the present work by the filler type and its content in the hydrogel.

Neat P(NIPAM-co-AA) hydrogels were also prepared following identical steps as for nanocomposite hydrogels without filler addition. **Fig. 1** illustrates the preparation of P(NIPAM-co-AA) nanocomposite hydrogels.

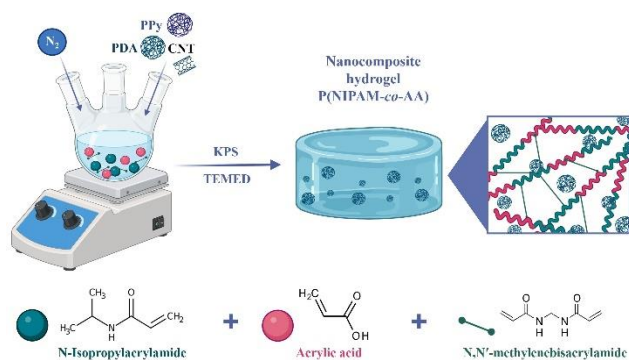


**Fig. 1.** Schematic representation of the preparation of P(NIPAM-co-AA) nanocomposite hydrogels.

## Characterization of materials

Attenuated total reflectance Fourier transformed infrared spectroscopy (ATR-FTIR) spectra were recorded on a Perkin-Elmer Frontier spectrometer equipped with a single reflection diamond accessory. Scanning electron microscopy (SEM) characterizations were performed using a JEOL JSM-5410LV microscope, operated with an acceleration voltage of 15 kV. The samples were gold-sputtered prior to SEM examination. Thermogravimetric analysis (TGA) was performed in a PerkinElmer Pyris 1 apparatus. Samples were heated at 10 °C min<sup>-1</sup> under a nitrogen atmosphere until 600 °C, followed by a gas switch to oxygen.

## Photothermal measurements of nanomaterials in suspension

A portion of 3 mL of PDA, PPy, or CNT suspensions in sodium phosphate buffer (pH 7.4, 100 mM) at different concentrations (8.88, 13.33, 17.77, 20, and 22.2  $\mu$ g mL<sup>-1</sup>) was irradiated with a laser (808 nm) Opto Engine PSU-III-LED for 10 min at 1 and 2 W cm<sup>-2</sup> of radiation power. Fluorescence quartz cells were used for all photothermal measurements. The distance between sample and NIR source was around 10 cm. The temperature of irradiated samples was recorded with a thermographic camera FLIR E53 24°. Measurements were performed in triplicate.

## Photothermal measurements of nanocomposite hydrogels

Cylindrical-shaped nanocomposite hydrogels of PDA, PPy, or CNT in hydrated state were placed inside fluorescence quartz cells. Similar photothermal measurements to those described in previous subsection were carried out in hydrogels. Control experiments were performed using filler-free hydrogels. Each sample was tested by triplicate.

## RESULTS AND DISCUSSION

### FTIR analysis

**Fig. 2** shows ATR-FTIR spectra of PDA, PPy, and CNT nanostructures. The spectrum of PDA nanoparticles shows a broad band from 3700 to 2800 cm<sup>-1</sup> due to the overlapping of signals corresponding to the stretching vibrations of hydroxyl and amine groups of dihydroxyindole moieties. The peak at 1734 cm<sup>-1</sup> is related to C=O stretching vibration of quinone structure and the band at 1550 cm<sup>-1</sup> is attributed to the absorption of the phenyl groups [27]. The peaks at 1365 cm<sup>-1</sup> and 1228 cm<sup>-1</sup> are due to bending vibrations of OH and CH<sub>2</sub> units of catechol groups, respectively [28].

The PPy spectrum displays the typical bands of this polymer. A broad band at 3600-3000 cm<sup>-1</sup> is due to the N-H symmetric stretching. Signals around 2920 and 2867 cm<sup>-1</sup> are attributed to C-H stretching vibrational modes. On the other hand, the C-C stretching vibration of the pyrrole ring is observed at 1553 cm<sup>-1</sup>. The peak at 1034 cm<sup>-1</sup> is due to the C-H in-plane deformation, whereas the C-H out-of-plane deformation band is observed at 933 cm<sup>-1</sup> [25].

The spectrum of CNT showed characteristic adsorption bands of functionalized nanotubes. The broad band located from 3500 to 3000 cm<sup>-1</sup> is due to the O-H stretching vibration. Signals of C=O, C-OH, and C-O stretching vibrations are also observed at 1690, 1414, and 1019 cm<sup>-1</sup>, respectively [29]. Signals of oxygenated groups in CNT-spectrum confirmed that the functionalization process was carried out successfully.

**Fig. 2** also includes ATR-FTIR spectra of P(NIPAM-co-AA) hydrogel and those of representative P(NIPAM-co-AA)/PDA, P(NIPAM-co-AA)/PPy, and P(NIPAM-co-AA)/CNT nanocomposite hydrogels. The spectrum of the P(NIPAM-co-AA) sample displays the typical absorptions

of its repeating units. The absorption band at  $3285\text{ cm}^{-1}$  can be assigned to the N-H stretching of the NIPAM units [30,31]. The bands at  $2970$  and  $2926\text{ cm}^{-1}$  are related to C-H vibrations of the methyl, methylene and methine groups. The presence of the AA units in the polymer chain is confirmed by the signal at  $1724\text{ cm}^{-1}$  attributed to the C=O stretching of the carboxyl units [32]. The strong band at  $1634\text{ cm}^{-1}$  is associated with the C=O stretching (amide I band) and the peak around  $1528\text{ cm}^{-1}$  is assigned to the N-H bending vibration (amide II band). The peak at  $1454\text{ cm}^{-1}$  is attributed to bending vibrations of -CH and -CH<sub>3</sub> groups, whereas the doublet at  $1384$  and  $1368\text{ cm}^{-1}$  is related to vibrations of groups -CH(CH<sub>3</sub>)<sub>2</sub>. Finally, the peak at  $1166\text{ cm}^{-1}$  is associated with the C-N stretching vibration [33].

The characteristic bands of P(NIPAM-co-AA) matrix dominate the IR spectra of nanocomposite hydrogels and the individual absorptions of PDA, PPy, CNT are not clearly distinguished. This feature may be due to the low concentration of nanostructures in hydrogel ( $1.2\text{ mg mL}^{-1}$ ) and the signal overlapping of different materials. However, spectral shifts and broadening of bands are detected in nanocomposite spectra with respect to that of neat hydrogel. Particularly, the signal of symmetric C-N vibration shifts to lower wavenumbers in the nanocomposite hydrogels spectra compared to its position in the P(NIPAM-co-AA) hydrogel spectrum. The spectral differences evidence the modification of the electronic environment of P(NIPAM-co-AA) chains by the filler presence.

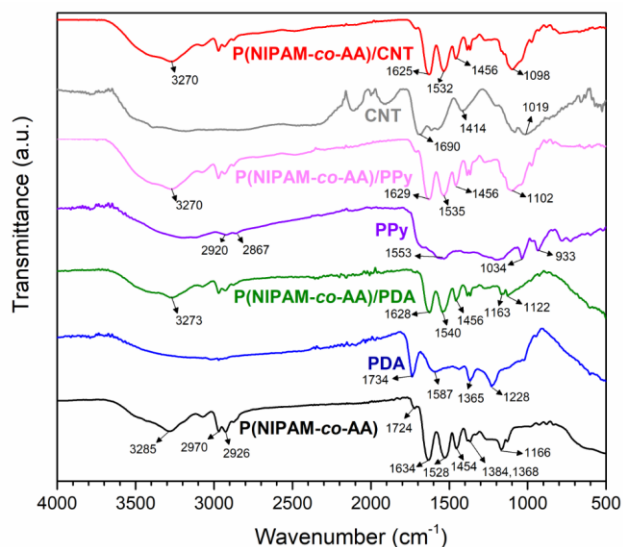


**Fig. 2.** ATR-FTIR spectra of PDA, PPy, and CNT nanomaterials and those of neat and nanocomposite P(NIPAM-co-AA) hydrogels.

### SEM analysis

**Fig. 3** shows the exterior appearance and internal microstructure of neat P(NIPAM-co-AA) network and those of P(NIPAM-co-AA)/PPy and P(NIPAM-co-AA)/CNT nanocomposite hydrogels. Images showed color changes of hydrogels by filler incorporation, evolving from

transparent to dark with PPy or CNT addition. At naked eye, PPy clusters were clearly distinguished within the transparent P(NIPAM-co-AA) matrix. This feature was also observed for P(NIPAM-co-AA)/PDA hydrogel (not shown). In contrast, no different phases were observed in P(NIPAM-co-AA)/CNT hydrogel at macroscopic scale; indicating that nanotubes were well dispersed within the 3D network. It should also be considered that CNT are low-density hollow structures that occupy a large volume of the network free space, giving rise to a more uniform black appearance of P(NIPAM-co-AA)/CNT hydrogel.

SEM images showed that all samples have an internal porous structure with defined boundaries. The incorporation of photothermal materials in the P(NIPAM-co-AA) matrix did not produce an apparent change in the network morphology since its porous and interconnected structure is maintained in both nanocomposite hydrogels. Furthermore, there are no significant differences in pore size between the different samples of hydrogels.

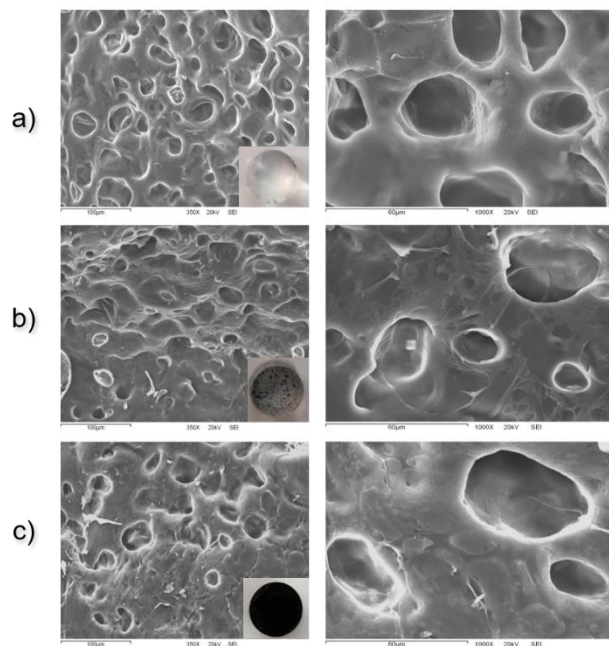


**Fig. 3.** SEM micrographs of cross sections of neat P(NIPAM-co-AA) hydrogel (a), as well as those of P(NIPAM-co-AA)/PPy (b) and P(NIPAM-co-AA)/CNT (c) nanocomposite hydrogels with  $1.2\text{ mg mL}^{-1}$  filler concentration.

### Thermal analysis

**Fig. 4** shows thermogravimetric (TG) curves of nanocomposite hydrogels and their corresponding first derivative thermogravimetric (DTG) curves with the indication of temperatures of maximum decomposition rate ( $T_{max}$ ). Thermal degradation of PNIPAM hydrogels is reported to occur in a single weight loss step, with  $T_{max}$  around  $410\text{ }^{\circ}\text{C}$  [34].

All nanocomposite samples showed a similar thermal degradation profile. Samples lost mass at temperatures below  $100\text{ }^{\circ}\text{C}$ , which was associated with the evaporation

of residual moisture. Individual polymer degradation steps overlap at temperatures above 100 °C. The first degradation step was observed from 120 to 180 °C with a  $T_{max}$  in the range 161–164 °C and a weight loss around 5.1–9.5 %. This loss was associated with the dehydration of carboxyl groups of the AA units [34]. The second decomposition step started around 230 °C and ended at 320 °C with  $T_{max}$  around 281–288 °C and weight loss of 15.3–18.4 %. For P(NIPAM-co-AA)/PPy hydrogels, this weight loss may be related to the degradation of low molecular weight chains of PPy. Orduño *et. al.* [35] reported that the  $T_{max}$  attributed to the PPy counterpart in PPy-containing hydrogels shifted to higher temperatures as compared to the value in its free form.

Finally, the third step of degradation around 345–450 °C with  $T_{max}$  of 370.5–382.9 °C and a weight loss of 92.6–94.1 % was mainly associated with the decomposition of P(NIPAM-co-AA) backbone.

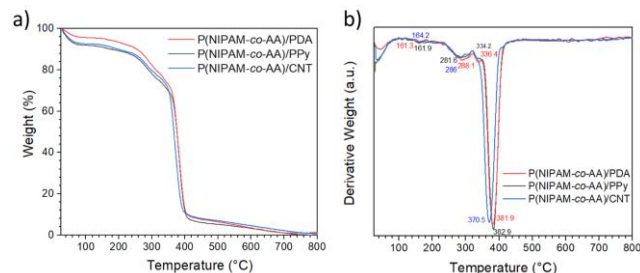


**Fig. 4.** Thermogravimetric (a) and first derivative curves (b) of P(NIPAM-co-AA)/PDA, P(NIPAM-co-AA)/PPy, and P(NIPAM-co-AA)/CNT nanocomposite hydrogels.

### Photothermal behavior

The photothermal properties of PDA, PPy, and CNT were studied under the same experimental conditions. **Fig. 5(a)** illustrates the experimental setup for thermal measurements of materials under NIR irradiation. The irradiation of light to the material induces reflection, dispersion, and absorption phenomena, the latter being the main responsible for the photothermal generation. In carbonaceous and polymer materials, the less tightly held electrons are promoted from the ground state (highest occupied molecular orbital, HOMO) to a higher energy orbital (lowest unoccupied molecular orbital, LUMO) upon irradiation with light energy that matches a possible electronic transition. The relaxation from the excited states to the ground states occurs by electron–phonon coupling. The energy is transferred from the excited electrons to vibrational modes within the atomic lattices, resulting in an increase of material temperature [36]. **Fig. 5(b)** displays a schematic illustration of photothermal mechanism in carbon- and polymer-based materials.

**Fig. 5(c)** shows results obtained in the analysis of photothermal effect of PDA suspensions at different concentrations ranging from 8.88 to 22.2  $\mu\text{g mL}^{-1}$ , irradiated with 1  $\text{W cm}^{-2}$  power during 10 min. Sodium phosphate buffer (pH 7.4) was used as a negative control. It is observed that the temperatures of all the PDA samples increased with the irradiation time, and with increasing the concentration of nanoparticles. For example, the temperature of the sample

with the lowest PDA content increased 8 °C after 10 min irradiation with 1  $\text{W cm}^{-2}$  power, while the sample with the highest PDA concentration reached 43 °C, increasing its temperature by 18 °C. In contrast, the temperature of buffer solution increased by only 1.5 °C in same conditions. This behavior confirmed the photothermal capacity of the synthesized PDA nanoparticles.

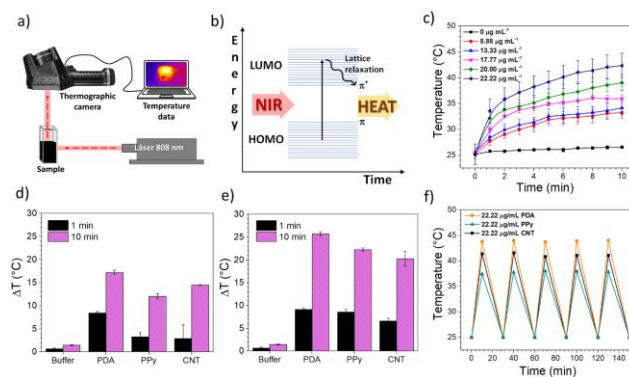


**Fig. 5.** Illustration of the experimental setup for photothermal measurements (a). Scheme of the photothermal conversion in carbon- and polymer-based materials (b). Thermal response of PDA suspensions of concentrations from 8.88 to 22.2  $\mu\text{g mL}^{-1}$  under 1  $\text{W cm}^{-2}$  power laser NIR irradiation (c). Temperature increments of PDA, PPy, and CNT suspensions of 22.2  $\mu\text{g mL}^{-1}$  concentration after 1 or 10 min of irradiation with 1 (d) and 2  $\text{W cm}^{-2}$  (e) power irradiation. Cycles of heating/cooling of PDA, PPy, and CNT suspensions of 22.2  $\mu\text{g mL}^{-1}$  concentration under alternating ON/OFF laser irradiation of 1  $\text{W cm}^{-2}$  power (f).

Additionally, it was found that the photothermal effect was sensitive to the power of laser, finding a more intense effect by increasing the power from 1 to 2  $\text{W cm}^{-2}$ . In this way, the 22.2  $\mu\text{g mL}^{-1}$  PDA suspension reached 50.8 °C after irradiation for 10 min at 2  $\text{W cm}^{-2}$ . **Fig. 5(d)** and **Fig. 5(e)** show the temperature changes of PDA, PPy, and CNT suspensions of 22.2  $\mu\text{g mL}^{-1}$  concentration after 1 or 10 min of irradiation with 1 and 2  $\text{W cm}^{-2}$  power irradiation, respectively. The effect was similar for three samples; higher irradiation times yield larger temperature increments whereas an increase of laser power from 1 to 2  $\text{W cm}^{-2}$  produces a more intense photothermal effect. Comparatively, PDA suspension showed larger temperature increases than PPy and CNT suspensions of similar concentration under same experimental conditions. The composition and structural characteristics of polymer nanoparticles depend on their synthesis conditions which, as the same time, determine their electronic nature and photothermal behavior. As mentioned earlier, experimental differences between photothermal studies lead to significant differences between the reported results for the same type of material. Therefore, by carrying out the measurements under same experimental conditions, the photothermal effect of different samples can be rigorously compared.

The three suspensions under 1  $\text{W cm}^{-2}$  of power laser reached temperatures in 39–43 °C range. This effect of mild hyperthermia can be used to produce membrane damages, inhibition of DNA synthesis and repair, cytoskeletal

damage, Na/K-ATP enzyme activation, etc. [24]. Furthermore, hyperthermia in the range of 47–50 °C at higher suspension concentrations, larger irradiation time, and laser power of 2 W cm<sup>-2</sup> can efficiently produce the ablation of malignant cells since cancer cells are thermally ablated after 15–60 min at 42 °C or above 50 °C in just 4–6 min [37]. Therefore, PDA, PPy, and CNT nanostructures are promising candidates to cancer therapy by thermo-induced coagulation necrosis of cancer tissues and/or cells.

To evaluate the photothermal stability of nanostructures in suspension, ON/OFF irradiation tests were performed. Fig. 5(f) shows the results of 5 cycles of ON/OFF laser illumination in 22.2 μg mL<sup>-1</sup> PDA, PPy, and CNT suspensions by using 1 W cm<sup>-2</sup> power. The samples were irradiated for 10 minutes, then allowed to cool for 20 minutes at room temperature, taking the temperature at the beginning and at the end of each cycle. The temperature variations were fully reversible within the tested conditions for the three samples, i.e., temperature increments stayed the same from one cycle to another. These ultimate results confirmed the potential of nanomaterials for PTT uses.

#### Photothermal effect of nanocomposite hydrogels

Fig. 6(a) shows the photothermal behavior of P(NIPAM-*co*-AA)/PDA nanocomposite hydrogel irradiated with 1 W cm<sup>-2</sup> laser power during 10 min. The thermal response of neat P(NIPAM-*co*-AA) hydrogel was also included as negative control since its temperature increased 1.4 °C after the NIR irradiation. The P(NIPAM-*co*-AA)/PDA hydrogel exhibited a similar behavior of those of PDA suspensions; the temperature increased with the PDA concentration and the time of NIR irradiation. These results confirmed that the PDA nanoparticles retained their photothermal capacity after being incorporated into P(NIPAM-*co*-AA) hydrogel.

Fig. 6(b) and Fig. 6(c) show the temperature increments of P(NIPAM-*co*-AA) hydrogel and those of P(NIPAM-*co*-AA)/PDA, P(NIPAM-*co*-AA)/PPy, and P(NIPAM-*co*-AA)/CNT nanocomposite hydrogels of 1.8 mg mL<sup>-1</sup> concentration after 1 or 10 min of NIR irradiation with 1 and 2 W cm<sup>-2</sup> power, respectively. As expected, the temperature rise of nanocomposite hydrogels was highly dependent on the irradiation time and the laser power. Moreover, it should be noticed that the thermal response of P(NIPAM-*co*-AA)/CNT hydrogel was more intense than those of P(NIPAM-*co*-AA)/PDA and P(NIPAM-*co*-AA)/PPy samples. This comparatively behavior was not consistent with the relative photothermal response of PDA, PPy, and CNT nanostructures in suspension (Fig. 5(d) and Fig. 5(e)). These results suggested that the photothermal behavior of composite materials is influenced not only by the inherent properties of the photothermal agents (photothermal efficiency, thermal conductivity, aspect ratio, density, etc.), but also by microstructural features such as the 3D distribution of nanostructures within the polymer matrix and the interactions between components of materials.

Fig. 6(d) shows thermographic images that qualitatively confirmed the high photothermal conversion

of nanocomposite hydrogels as compared with the poor response of neat hydrogel. Overall, the photothermal assessment of P(NIPAM-*co*-AA) hydrogels filled with PDA, PPy, and CNT nanostructures demonstrated the potential of these materials for NIR-based PTT applications, either to suppress the growth of cancer cells or for the controlled release of chemotherapeutic drugs. The carboxyl side groups of P(NIPAM-*co*-AA) matrix provide an additional affinity under mild conditions to positively charged drugs, such as anthraquinone chemotherapeutics, promoting the drug-loading capacity of material [24]. Furthermore, the photothermal conversion can induce a volumetric phase change of nanocomposite hydrogels due to the thermosensitive nature of its P(NIPAM-*co*-AA) matrix [38,39]. In this sense, Ramírez *et al.* [38], carried out temperature-dependent swelling measurements of P(NIPAM-*co*-AA) hydrogels to determine their volume phase transition temperature (VPTT). The results showed a clear volume phase transition of P(NIPAM-*co*-AA) matrix between 43 and 52 °C. The P(NIPAM-*co*-AA) matrix swells in aqueous media below its VPTT, and above this critical temperature, the 3D structure contracts. This thermosensitive effect of P(NIPAM-*co*-AA)-based hydrogels have been successfully used for controlled/sustained drug delivery applications [30,40].

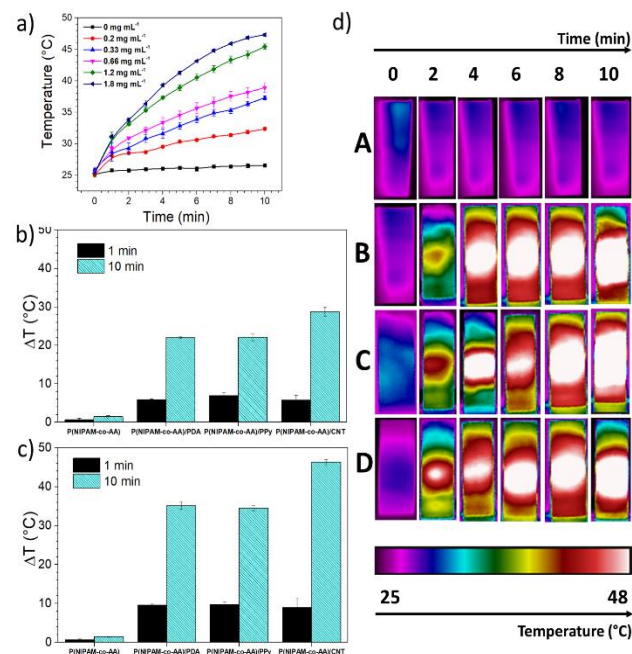


Fig. 6. Thermal response of P(NIPAM-*co*-AA)/PDA nanocomposite hydrogel of PDA concentrations from 0.2 to 1.8 mg mL<sup>-1</sup> under 1 W cm<sup>-2</sup> power laser NIR irradiation (a). Temperature increments of P(NIPAM-*co*-AA) hydrogel and those of P(NIPAM-*co*-AA)/PDA, P(NIPAM-*co*-AA)/PPy, and P(NIPAM-*co*-AA)/CNT nanocomposite hydrogels of 1.8 mg mL<sup>-1</sup> filler concentration after 1 or 10 min of NIR irradiation with 1 (b) and 2 W cm<sup>-2</sup> (c) power irradiation. Thermographic images of P(NIPAM-*co*-AA) (A) hydrogel and those of P(NIPAM-*co*-AA)/PDA (B), P(NIPAM-*co*-AA)/PPy (C), and P(NIPAM-*co*-AA)/CNT (D) nanocomposite hydrogels of 1.2 mg mL<sup>-1</sup> filler concentration under NIR irradiation with 1 W cm<sup>-2</sup> power (d).

## CONCLUSION

The comparative analysis of synthesized PDA and PPy nanoparticles, as well as that of chemically modified CNT, showed that all samples exhibited a reversible photothermal effect in buffer suspension. The PDA suspension exhibited a higher photothermal conversion than PPy and CNT suspensions of similar concentration under same experimental conditions. All nanomaterials retained their photothermal capacity after being incorporated into a P(NIPAM-co-AA) hydrogel. The photothermal effect of nanoparticles suspensions and nanocomposite hydrogels was highly dependent on the nanostructure concentration, the irradiation time, and the laser power. The thermal response of P(NIPAM-co-AA)/CNT hydrogel under NIR radiation was more intense than those of P(NIPAM-co-AA)/PDA and P(NIPAM-co-AA)/PPy hydrogels, which was related with the large volume occupied by the well-dispersed hollow nanotubes within the hydrogel. The photothermal properties of nanocomposite hydrogels render these multifunctional polymer systems as potential candidates for their application in controlled release of drugs and synergistic chemo-photothermal therapy against cancer cells through NIR laser irradiation.

## ACKNOWLEDGEMENTS

This research was supported by the Consejo Nacional de Humanidades, Ciencias y Tecnologías (CONAHCYT), Mexico, Grant number A1-S-26204, Ciencia Básica 2017–2018. Gabriela Herrera-Rodríguez, Andya Jhosephin Ramírez Irigoyen, Karla Fabiola García Verdugo, Ana Valeria Torres Figueroa, and Brianda Maria Salazar Salas acknowledge CONAHCyT for their scholarships during this study. The authors thank Dr. Irela Santos Saucedo for the thermal analysis, Dr. Silvia Elena Burruel Ibarra for SEM examinations, and Prof. Angel Benjamín Gutierrez Cureño for the construction of laser assembly.

## CONFLICTS OF INTEREST

There are no conflicts to declare.

## REFERENCES

- Xiao, L.; Chen, X.; Yang, X.; Sun, J.; Geng, J.; *ACS Appl. Polym. Mater.*, **2020**, *2*, 4273. <https://dx.doi.org/10.1021/acsapm.0c00711>
- Wu, X.; Chen, G. Y.; Owens, G.; Chu, D.; Xu, H.; *Mater. Today Energy.*, **2019**, *12*, 277. <https://doi.org/10.1016/j.mtener.2019.02.001>
- Chen, H.; Shi, R.; Zhang, T.; *Molecules.*, **2021**, *26*, 7752. <https://doi.org/10.3390/molecules26247552>
- Ibrahim, I.; Seo, D. H.; McDonagh, A. M.; Shon, H.K.; Tijing, L.; *Desalination.*, **2021**, *500*, 114853. <https://doi.org/10.1016/j.desal.2020.114853>
- Mirza-Aghayan, M.; Heidarian, M.; Mohammadi, M.; Boukheroub, R.; *Appl. Surf. Sci.*, **2022**, *583*, 152568. <https://doi.org/10.1016/j.apsusc.2022.152568>
- Wang, H.; Chang, J.; Shi, M.; Pan, W.; Li, N.; Tang, B.; *Angew. Chem.* **2019**, *131*, 1069. <https://doi.org/10.1002/ange.201811273>
- Han, J.; Feng, Y.; Liu, Z.; Chen, Q.; Shen, Y.; Feng, F.; Liu, L.; Zhong, M.; Zhai, Y.; Bockstaller, M.; Zhao, Z.; *Polymer.*, **2021**, *230*, 124018. <https://doi.org/10.1016/j.polymer.2021.124018>
- Liu, B.; Sun, J.; Zhu, J.; Li, B.; Ma, C.; Gu, X.; Liu, K.; Zhang, H.; Wang, F.; Su, J.; Yang, Y.; *Adv. Mater.*, **2020**, *32*, 2004460. <https://doi.org/10.1002/adma.202004460>
- Wei, W.; Zhang, X.; Zhang, S.; Wei, G.; Su, Z.; *Mater. Sci. Eng. C.*, **2019**, *104*, 109891. <https://doi.org/10.1016/j.msec.2019.109891>
- Toci, G.; Olgianti, F.; Pallavicini, P.; Fernandez, Y.A.D.; De Vita, L.; Dacarro, G.; Grisoli, P.; Taglietti, A.; *Nanomaterials.*, **2021**, *11*, 3252. <https://doi.org/10.3390/nano11123252>
- Jiang, H.; Xing, Z.; Zhao, T.; Yang, Z.; Wang, K.; Li, Z.; Yang, S.; Xie, L.; Zhou, W.; *Appl. Catal. B Environ.*, **2020**, *274*, 118947. <https://doi.org/10.1016/j.apcatb.2020.118947>
- Lagos, K. J.; Buzzá, H. H.; Bagnato, V. S.; Romero, M. P.; *Int. J. Mol. Sci.*, **2022**, *23*, 22. <https://doi.org/10.3390/ijms23010022>
- Jung, H. S.; Verwilt, P.; Sharma, A.; Sessler, J. L.; Seung, J.; *Chem Soc Rev.*, **2018**, *47*, 2280. <https://doi.org/10.1039/c7cs00522a>
- Vines, J. B.; Lim, D.; Park, H.; *Polymer.*, **2018**, *10*, 1357. <https://doi.org/10.3390/polym10121357>
- Sharifi, S.; Behzadi, S.; Laurent, S.; Forrest, M. L.; Stroeve, P.; Mahmoudi, M.; *Chem. Soc. Rev.* **2012**, *41*, 2323. <https://doi.org/10.1039/c1cs15188f>
- Wang, X.; Wang, C.; Cheng, L.; Lee, S.T.; Liu, Z.; *J. Am. Chem. Soc.*, **2012**, *134*, 7414. <https://doi.org/10.1021/ja300140c>
- Mahajan, S.; Patharkar, A.; Kuche, K.; Maheshwari, R.; Deb, P. K.; Kalia, K.; Tekade, R. K.; *Int. J. Pharm.*, **2018**, *548*, 540. <https://doi.org/10.1016/j.ijpharm.2018.07.027>
- Serhan, M.; Sprowls, M.; Jackemeyer, D.; Long, M.; Perez, I. D.; Maret, W.; Tao, N.; Forzani, E.; *J. Mater. Chem. B.*, **2019**, *8*, 1–11. <https://doi.org/10.1039/C4TB01738B>
- Li, W.; Wang, X.; Wang, J.; Guo, Y.; Lu, S.Y.; Li, C.M.; Kang, Y.; Wang, Z.G.; Ran, H.T.; Cao, Y.; Liu, H.; *Biomac.*, **2019**, *20*, 401. <https://doi.org/10.1021/acs.biomac.8b01453>
- Guillet, J. F.; Flahaut, E.; Golzio, M.; *ChemPhysChem.*, **2017**, *18*, 2715. <https://doi.org/10.1002/cphc.201700517>
- Liu, C.; Ma, Y.; Guo, S.; He, B.; Jiang, T.; *Biomater. Sci.*, **2021**, *9*, 4356. <https://doi.org/10.1039/d0bm01766c>
- Zhao, J.; Xu, W.; Zhao, Z.; Ling, G.; Zhang, P.; *Composites. Part B Eng.*, **2022**, *243*, 110130. <https://doi.org/10.1016/j.compositesb.2022.110130>
- Wang, X.; Wang, C.; Wang, X.; Wang, Y.; Zhang, Q.; Cheng, Y.; *Chem. Mater.*, **2017**, *29*, 1370. <https://doi.org/10.1021/acs.chemmater.6b05192>
- Geng, S.; Zhao, H.; Zhan, G.; Zhao, Y.; Yang, X.; *ACS Appl. Mater. Interfaces.*, **2020**, *12*, 7995. <https://doi.org/10.1021/acsami.9b22654>
- Grijalva Bustamante, G. A.; Quevedo Robles, R. V.; Del Castillo Castro, T.; Castillo Ortega, M. M.; Encinas, J. C.; Rodríguez-Félix, D. E.; Lara Cenicerros, T. E.; Fernández Quiroz, D.; Lizardi Mendoza, J.; Armenta Villegas, L. *Colloids and Surfaces*, **2020**, *600*, 124961. <https://doi.org/10.1016/j.colsurfa.2020.124961>
- Quevedo-Robles, R. V.; Grijalva-Bustamante, G. A.; Del Castillo-Castro, T.; Castillo-Ortega, M. M.; Rodríguez-Félix, D. E.; Lara Cenicerros, T. E.; Mayen-Mondragon, R.; Santos Saucedo, I.; *Synth. Met.*, **2019**, *253*, 100. <https://doi.org/10.1016/j.synthmet.2019.05.006>
- Sun, G.; Zu, F.; Koch, N.; Rappich, J.; Hinrichs, K.; *Phys. Status Solidi B.*, **2019**, *256*, 1800308. <https://doi.org/10.1002/pssb.201800308>
- Rahoui, N.; Hegazy, M.; Jiang, B.; Taloub, N.; Huang, Y. D.; *Am. J. Anal. Chem.*, **2018**, *09*, 273–285. <https://doi.org/10.4236/ajac.2018.95021>
- Zeng, W. J.; Li, C.; Feng, Y.; Zeng, S. H.; Fu, B. X.; Zhang, X. L.; *J. Water Process Eng.*, **2021**, *40*, 101901. <https://doi.org/10.1016/j.jwpe.2020.101901>
- Shin, H. H.; Choi, H. W.; Lim, J. H.; Kim, J. W.; Chung, B. G.; *Nanoscale Res. Lett.*, **2020**, *15*. <https://doi.org/doi.org/10.1186/s11671-020-03444-4>
- Wang, W.; Narain, R.; Zeng, H.; *Polymer Science and Nanotechnology*, **2020**. [https://doi.org/https://doi.org/10.1016/B978-0-12-816806-6.00010-8\\_203](https://doi.org/https://doi.org/10.1016/B978-0-12-816806-6.00010-8_203)
- Shin, H. H.; Choi, H. W.; Lim, J. H.; Kim, J. W.; Chung, B. G.; *Nanoscale Res Lett.*, **2020**, *15*, 214. <https://doi.org/10.1186/s11671-020-03444-4>
- Farooqi, Z. H.; Khan, H. U.; Shah, S. M.; Siddiq, M.; *Arab. J. Chem.*, **2017**, *10*, 329. <https://doi.org/10.1016/j.arabjc.2013.07.031>
- Torres-Figueroa, A. V.; Pérez-Martínez, C. J.; Encinas, C. J.; Burruel-Ibarra, S.; Silvas-García, M. I.; García Alegría, A. M.; Del Castillo-Castro, T.; *Pharmaceutics.*, **2021**, *13*, 1284. <https://doi.org/10.3390/pharmaceutics13081284>

35. Orduño Rodríguez, A. M.; Pérez-Martínez, C. J.; Del Castillo Castro, T.; Castillo Ortega, M. M.; Rodríguez-Félix, D. E.; Romero García, J.; *Polym. Bull.*, **2019**, *77*, 1217.  
https://doi.org/10.1007/s00289-019-02788-x
36. Tee, S. Y.; Win, K. Y.; Goh, S. S; Teng, C. P.; Tang, K. Y.; Regulacio, M. D.; Li, Z.; Ye, E.; Introduction to Photothermal Nanomaterials; Ye, E.; Li, Z. (Eds.); The Royal Society of Chemistry, Reino Unido, **2022**, pp. 1–32.  
https://doi.org/10.1039/9781839165177-00001
37. Liu, Y.; Ai, K.; Liu, J.; Deng, M.; He, Y.; Lu, L.; *Adv. Mater.*, **2013**, *25*, 1353. https://doi.org/10.1002/adma.201204683
38. Ramírez-Irigoyen, A. J.; García-Verdugo, K. F.; Castillo-Ortega, M. M.; Rodríguez-Félix, D. E.; Encinas, J. C.; Plascencia-Jatomea, M.; Argüelles-Monal, W.; Saucedo, I. S.; Pérez-González, R.; del Castillo-Castro, T.; *J. Appl. Polym. Sci.*, **2023**, 1-12.  
https://doi.org/10.1002/app.54338.
39. Kojima, H.; *Polym. J.*, **2018**, *50*, 411–418.  
https://doi.org/10.1038/s41428-018-0035-9.
40. Wan, J.; Geng, S.; Zhao, H.; Peng, X.; Xu, J.; Wei, M.; Mao, J.; Zhou, Y.; Zhu, Q.; Zhao, Y.; Yang, X.; *Nanoscale.*, **2018**, *10*, 20020.  
https://doi.org/10.1039/c8nr06851h

### AUTHORS BIOGRAPHY



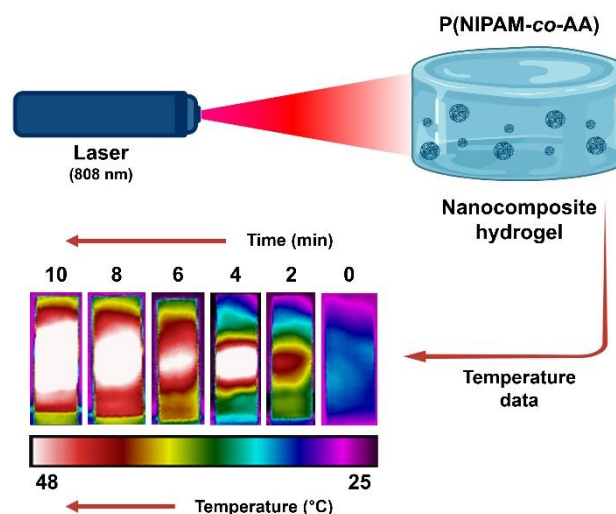
**Cinthia Jhovanna Pérez Martínez** Ph.D. is a Professor in the Department of Biological Chemical Sciences of the University of Sonora, recognized as a Level 1-National Researcher by CONAHCYT, Mexico. Her research activity is focused on projects related to polymers for biomedical applications such as release of biomolecules, publishing several scientific articles in indexed journals.



**Teresa del Castillo Castro** Ph.D. is a Titular Professor of the Department of Research in Polymers and Materials of the University of Sonora, recognized as a Level 2 National Researcher by CONAHCYT, Mexico. Her research activity is focused on stimuli-responsive polymer systems for biomedical applications.

### GRAPHICAL ABSTRACT

The photothermal behavior of poly(N-isopropylacrylamide-co-acrylic acid) hydrogels containing polydopamine, polypyrrole, or carbon nanotubes was comparatively studied under the same experimental setup.



This article is licensed under a Creative Commons Attribution 4.0 International License, which allows for use, sharing, adaptation, distribution, and reproduction in any medium or format, as long as appropriate credit is given to the original author(s) and the source, a link to the Creative Commons license is provided, and changes are indicated. Unless otherwise indicated in a credit line to the materials, the images or other third-party materials in this article are included in the article's Creative Commons license. If the materials are not covered by the Creative Commons license and your intended use is not permitted by statutory regulation or exceeds the permitted use, you must seek permission from the copyright holder directly.

Visit <http://creativecommons.org/licenses/by/4.0/> to view a copy of this license.